Q-adaptive deconvolution

Dave Hale

Abstract

An adaptive seismic deconvolution algorithm based on and constrained by a physical model of attenuation is proposed as an alternative to more conventional, time-varying deconvolution methods. Q-adaptive deconvolution (QAD) requires an iterative application of conventional prediction error filtering and inverse Q-filtering, with the former process aimed at source, receiver, and near-surface reverberations and the latter compensating for attenuation effects. With special consideration given to the possible over-amplification of high-frequency noise, a "clipped" inverse Q-filter is described as particularly appropriate for QAD.

We compare QAD with conventional deconvolutions through application to field recorded seismograms. QAD more effectively compensates for the attenuation of high-frequencies and dispersion effects while yielding estimates of the quality factor Q and avoiding the windowing or weighting of seismograms required by conventional methods.

Introduction

The convolutional model for seismic data is that each seismic trace is the convolution of a "source waveform", including near-surface reverberations and receiver distortions, with the earth's subsurface impulse response. We would indeed be fortunate if that impulse response were a stationary, uncorrelated reflection coefficient sequence, for then both the source waveform and the reflection coefficients might be computed statistically using conventional deconvolution processes. We are never so lucky. The earth's impulse response contains much more than the desired reflection coefficient sequence; inter- and intra-bed multiples and inelastic attenuation are commonly observed contaminants which cause samples of the impulse response to be correlated in a particularly troublesome, non-stationary way.

Non-stationarity is typically circumvented windowing or weighting of seismograms. In the simplest approach, one divides a seismic trace into several overlapping windows, deconvolves each separately, and then blends the windows together to form a deconvolved trace. The choice of window length is rather important and has been discussed in detail by several authors, including Foster et al (1968) and Wang (1969). For any window length, however, the implied assumption of piecewise stationarity is inconsistent with physical models for multiples and attenuation.

Adaptive deconvolution methods, as described by Widrow (1970), Griffiths et al (1977), or Lee et al (1981), may provide a favorable alternative to windowing; a continuously time-varying deconvolution filter obviates the blending of windows. However, these adaptive methods are actually just efficient algorithms for windowing as above, but with a new weighting (essentially windowing) of data for every computed output sample. The user-specified adaptation rate required by these methods is analogous to the window length required in the simple approach.

Windowing or weighting of data is undesirable, not only because it requires a user-specified window length or adaptation rate, but also because it forces us to neglect useful information about the source waveform (including near-surface and recording distortions) contained throughout the seismogram. The non-stationarity of seismograms lies in the earth's impulse response, not in the source waveform; hence, the entire seismogram should be used in estimating the latter. Furthermore, the common assumption that reflection coefficients are uncorrelated (the "whiteness" assumption) is made less valid by weighting.

One way to avoid weighting is to incorporate a physical model for non-stationarity in the deconvolution process. An earlier paper by Hale (1981b) describes a Q-adaptive deconvolution (QAD) method based on and constrained by a model for inelastic attenuation. QAD compared favorably with more conventional adaptive methods when applied to synthetic

seismograms. This paper extends that work by first discussing the relative merits of various inverse Q-filtering (IQF) algorithms. An IQF is any time-variable filter which removes the effects of attenuation and is, naturally, a key ingredient of QAD. An IQF algorithm suggested by Fabio Rocca (1981) is shown to be particularly efficient for QAD. Finally, we demonstrate the merits of QAD with an application to field data.

Methods of inverse Q-filtering

The seismogram model on which our deconvolution method is based is represented by the following equations:

$$X(f) = \int dt\, e^{-2\pi i f t}\, e^{-\frac{\pi t}{Q}[|f| + iH(|f|)]}\, r(t) \tag{1a}$$

$$Y(f) = W(f)\, X(f) \tag{1b}$$

where $r(t)$ is the impulsive point-source response for a non-attenuating earth, $H(|f|)$ is the Hilbert transform of $|f|$, Q is the quality factor assumed constant, $X(f)$ is the impulsive point-source response for an attenuating earth, $W(f)$ is the source waveform, and $Y(f)$ is the seismic trace. $Y(f)$, $W(f)$, and $X(f)$ are frequency domain functions; i.e., $Y(f)$ is the Fourier transform of the time-domain seismogram $y(t)$. SEP-26 (Hale, 1981a) contains an equivalent matrix representation of this model.

We assume that $r(t)$ is the desired output from the deconvolution process, even though $r(t)$ must contain multiple reflections. The problem of estimating reflection coefficients from $r(t)$ is beyond the scope of this paper.

How then do we compute $r(t)$? Suppose we have recorded $y(t)$ and we somehow know $W(f)$ and Q as well. Inversion of equation (1b) is trivial provided $|W(f)|$ is nowhere zero. But to compute $r(t)$ from $X(f)$, we need the inverse of the relatively awkward transform (1a). A first guess might be

$$\tilde{r}(t) \equiv \int df\, e^{2\pi i f t}\, e^{+\frac{\pi t}{Q}G(f)}\, X(f) \tag{2}$$

where we have defined $G(f) \equiv |f| + iH(|f|)$. This guess is certainly correct in the limit of no attenuation, $Q = \infty$; but, in general,

$$\tilde{r}(t) = \int du\, r(u)\, v(t-u)$$

where

$$v(t) \equiv \int df\, e^{2\pi i f t}\, e^{+\frac{\pi t}{Q}G(f)}$$

In other words, $\tilde{r}(t) = r(t)$ only when $Q = \infty$. A method for exactly inverting equation (1a) is given in SEP-26 (Hale, 1981a). In practice, however, because $v(t)$ is (for typical $Q \approx 100$) almost a delta function, one may use the approximate inverse transform (2) without notable error.

Inverse Q-filtering (IQF), as represented by equation (2), may seem to be a rather expensive process, requiring a frequency domain integration for each time t. For a seismogram of N samples, the implied computational cost is proportional to N^2. Cheaper IQF algorithms may be derived by replacing the frequency-domain integrations with time-domain integrations. For example, equation (2) may be rewritten as

$$\tilde{r}(t) = \int df\ e^{2\pi i f t} \left[e^{\frac{\pi}{Q} G(f)} \right]^t X(f)$$

Defining $p(t)$ to be the inverse Fourier transform of the function in brackets, use of the convolution theorem yields

$$\tilde{r}(t) = \int du\ x(t-u)\, p^{*t}(u) \tag{3}$$

where p^{*t} denotes the tth convolutional power of p. The recursion $p^{*t} = p^{*(t-1)} * p$ and the fact that $p(t)$ may be approximated by a rather short (length $\ll N$) filter make implementation of equation (3) considerably cheaper than direct implementation of equation (2).

In addition to increased efficiency, the interpretation (3) of equation (2) leads to a Kalman filtering approach to the deconvolution of data contaminated with ambient noise (Hale, 1981c) as well as to a method for Q-adaptive deconvolution (Hale, 1981b). For the latter process, however, an alternative IQF algorithm suggested by Fabio Rocca (1981) is particularly efficient.

Rocca's suggestion is to rewrite equation (2) as

$$\tilde{r}(t) \equiv \int df\ e^{2\pi i f t} X(f) \left[1 + \frac{\pi t}{Q} G(f) + \frac{1}{2!} \left(\frac{\pi t}{Q} \right)^2 G^2(f) + \cdots \right]$$

Defining $g(t)$ to be the inverse Fourier transform of $G(f)$ and using the convolution theorem,

$$\tilde{r}(t) = x(t) + \frac{\pi t}{Q} [g(t) * x(t)] + \frac{1}{2!} \left(\frac{\pi t}{Q} \right)^2 [g(t) * g(t) * x(t)] + \cdots \tag{4}$$

$$= \sum_{j=0}^{\infty} \frac{1}{j!} \left(\frac{\pi t}{Q} \right)^j [g^{*j}(t) * x(t)]$$

The number of terms required to make the error in the Maclaurin series negligible depends on the ratio t/Q; but, for a given Q, the computational costs of equations (3) and (4) are

roughly equal. Note, however, that most of the work in computing $\tilde{r}(t)$ via equation (4) lies in convolving $g(t)$ with $x(t)$ repeatedly. Because this work may be done independent of Q, the cost of using equation (4) twice for different values of Q is much less than that of using equation (3) twice, provided one saves the $g^{*j}(t) * x(t)$. The reduction in computations may be considerable in any Q-estimation process, such as QAD described in SEP-28 (Hale, 1981b), which iteratively estimates Q by applying IQF for different Q until some function is minimized.

The required discrete form g_t of the filter $g(t)$ is shown in the appendix to be

$$g_t = \begin{cases} 1/4 & , \ t = 0 \\ -2/(\pi t)^2 & , \ t = 1,3,5, \cdots \\ 0 & , \ otherwise \end{cases} \tag{5}$$

The filter coefficients decay quickly enough so that finite-length (≈ 10) approximations may be used with negligible error.

Q-adaptive prediction error filtering

Q-adaptive deconvolution as presented in SEP-28 is a modification of more conventional, time-invariant, unit-lag prediction error filtering (PEF). Simply stated, both Q and the source-waveform $w(t)$ are estimated to minimize a sum of squared prediction errors. Given an efficient IQF algorithm, one can certainly imagine alternative functions to minimize. We justify our choice of summed, squared prediction errors by noting that (1) PEF is currently one of the most widely-used deconvolution methods, (2) the implied minimum-phase assumption is at least satisfied by our attenuation model, if not the source waveform $w(t)$, and (3) even if $w(t)$ is not minimum-phase, the minimum-phase estimate provided by PEF is usually a good initial estimate for use in iterative deconvolution methods which make no phase assumptions (e.g., minimum-entropy deconvolution).

The derivation of QAD in SEP-28 was based on the IQF algorithm of equation (3). An alternative derivation is possible via equation (4). Assume for now that we have already deconvolved the source waveform w_t from the seismogram y_t to obtain x_t. (For simplicity, we henceforth use discrete time functions, denoted by subscripts, rather than the continuous time functions used earlier. The sampling interval is assumed to be unity.) Following the derivation of conventional, unit-lag PEF, we might think of $\tilde{r}(t)$ (or its discrete version $\tilde{r}_t$) in equation (4) as the prediction error and choose Q (or, equivalently, Q^{-1}) to minimize

$$E(Q^{-1}) \equiv \sum_{t=1}^{N} \tilde{r}_t^2$$

The obviously unrealistic solution, however, is $Q^{-1} = -\infty$. The problem lies in the fact that IQF can significantly alter the amplitude of $\tilde{r}_t$. As is perhaps best seen from equation (2), $Q^{-1} = -\infty$ yields $\tilde{r}_t = 0$ for recorded time $t > 0$, thereby minimizing $E(Q^{-1})$.

A more reasonable function to minimize is

$$E(Q^{-1}) \equiv \sum_{t=1}^{N} e_t^2 \tag{6a}$$

where

$$e_t \equiv e^{-\frac{\pi t g_0}{Q}} \tilde{r}_t = e^{-\frac{\pi t}{4Q}} \tilde{r}_t \tag{6b}$$

Substituting for $\tilde{r}_t$ from equation (4), one can verify that unit weight is applied to x_t in computing e_t. In other words, the leading coefficient of the amplitude normalized IQF is constrained to be unity, independent of Q. This constraint (which is also imposed in conventional PEF where the first coefficient of the prediction error filter is unity) eliminates trivial, unrealistic solutions to the problem of minimizing $E(Q^{-1})$. The solution must now depend on x_t.

Given the function $E(Q^{-1})$ defined by equations (6), how does one compute the minimizing Q^{-1}? First, note that we have defined E to be a function not of Q but of Q^{-1}; this definition is intended to make the following derivation less cumbersome. To simplify notation, we define the new variable $\gamma \equiv Q^{-1}$. Secondly, note that e_t as defined by equations (4) and (6b) is a non-linear function of γ. Therefore, the equation $dE/d\gamma = 0$ is non-linear in γ. We shall solve this equation for γ by iteration. Define a current estimate $\bar{\gamma}$ and a perturbation $\Delta\gamma$ by $\gamma = \bar{\gamma} - \Delta\gamma$. Then

$$E(\Delta\gamma) \equiv \sum_t e_t^2(\gamma) \approx \sum_t \left[e_t(\bar{\gamma}) - \Delta\gamma \frac{de_t}{d\gamma}(\bar{\gamma}) \right]^2$$

and the minimizing $\Delta\gamma$ is

$$\Delta\gamma = \frac{\sum_t e_t \frac{de_t}{d\gamma}}{\sum_t \left(\frac{de_t}{d\gamma} \right)^2} \tag{7}$$

The iteration implied by these equations is roughly (but not quite) Newton's method for finding a zero of a non-linear function.

A good approximation to the required derivative $de_t/d\gamma$ may be found from equations (4) and (6b):

$$\frac{de_t}{d\gamma} \approx \pi t[(g_t - g_0\delta_t) * e_t] \approx -\frac{2t}{\pi} e_{t-1} \tag{8}$$

The latter approximation, justified by the definition of g_t in equation (5), yields the following equation for the perturbation

$$\Delta\gamma = -\frac{\pi}{2} \frac{\sum_t t e_t e_{t-1}}{\sum_t t^2 e_{t-1}^2} \tag{9}$$

Equation (9) is equivalent, excepting differences in notation, to equation (11) of SEP-28. We expect this equivalence because equations (3) and (4) are equivalent; our criteria for estimating γ (i.e., that $\Delta\gamma = 0$) must not depend on our choice between two equivalent IQF algorithms.

Recall our earlier assumption that x_t is the result of deconvolving the source waveform w_t from y_t. Because w_t is typically unknown, QAD must iteratively estimate w_t along with γ. The following iterative algorithm was proposed in SEP-28.

Initially $\gamma = \bar{\gamma}$, and y_t is a divergence-corrected seismogram

(1) $x_t = IQF(y_t)$

(2) $r_t = PEF(x_t)$

(3) $\Delta\gamma = -\frac{\pi}{2} \frac{\sum_t t r_t r_{t-1}}{\sum_t t^2 r_{t-1}^2}$

(4) $\gamma = \gamma - \Delta\gamma$

(5) If $|\Delta\gamma| > small$ go to (1)

Converged r_t is the deconvolved seismogram

PEF in step (2) of the algorithm is the conventional, unit-lag, prediction error filtering subroutine. Because PEF is a statistical process which performs best on stationary data, we apply PEF after IQF, even though the model of equations (1) implies that the source waveform must be deconvolved before IQF. In fact, according to our model, the spherical divergence correction (effectively conversion of a point-source response to a plane-wave response) must be performed after both PEF and IQF. The problem is that time-varying filters do not commute; however, because IQF and divergence correction are typically only weakly time-varying, the error in assuming commutativity is usually negligible, particularly if a short prediction error filter is used in step (2).

Note that in step (3) we have not bothered to compute the exponentially damped e_t of equation (9), but have used the undamped r_t instead. Aside from avoiding some

computation, use of r_t speeds convergence of the algorithm by placing more emphasis on the later samples of r_t where attenuation has its greatest effect. Application of the above QAD algorithm to synthetic traces in SEP-28 demonstrated convergence in about six iterations to a correct $\gamma \approx 0.01$, starting from an initial guess of $\gamma = 0$.

QAD as outlined above is an intuitively reasonable process. Conventional, unit-lag PEF computes L prediction error filter coefficients such that

$$\sum_t r_t r_{t-\tau} = 0 \quad ; \tau = 1, 2, 3, \cdots, L \tag{10}$$

QAD computes one more parameter, γ, by further requiring that

$$\sum_t t r_t r_{t-1} = 0 \tag{11}$$

If the input seismogram were stationary, then equations (10) for $\tau = 1$ would imply equation (11); and γ would equal zero -- no attenuation. When attenuation is present, however, the temporal averages in equations (10) are not equivalent to the desired ensemble averages; equations (10) then do not imply equation (11), and the simultaneous satisfaction of conditions (10) and (11) enhances the stationarity of the output r_t. Because attenuation produces a smooth, exponential spectral trend, the first lag of the autocorrelation ($\tau = 1$) is most sensitive to changes in γ and, hence, plays the most important role in these equations.

Clipped inverse Q-filtering for noisy (real) seismograms

The success of QAD in deconvolving computer generated synthetic seismograms is encouraging, but the effectiveness of QAD applied to field recorded seismograms must depend on the validity of our model given by equations (1). Although this model is closer to reality than are models which ignore attenuation, one obvious shortcoming is the omission of ambient noise. In conventional PEF, we inhibit the inversion of the source waveform at noise-dominated frequencies, typically by "pre-whitening" the autocorrelation of a seismogram. Effectively, the gain applied by PEF to any spectral component is limited to a maximum value.

A similar method for limiting or clipping the gain of an IQF is required for practical application of QAD to real seismograms. For example, one can easily show that the unclipped IQF of equations (2), (3), or (4) amplifies the Nyquist frequency by a factor of $\approx 7 \times 10^6$ when $t/Q \approx 10$. For typical $Q \approx 100$ and typical seismogram lengths greater than 1000 samples, seismic data is seldom pure enough to warrant the use of unclipped IQF.

As shown in the appendix, one may achieve clipped IQF by replacing the convolutions $g_t * x_t$ in equation (4) with

$$\sum_{s=0}^{\infty} g_{ts}\, x_{t-s}$$

The analogous replacement is required for $g_t * (g_t * x_t)$, etc. The time-variable filter g_{ts} is defined by

$$g_{ts} \equiv \begin{cases} 0 & , s < 0 \\ a_t(1-a_t) & , s = 0 \\ -2\sin^2(\pi a_t s)/(\pi s)^2 & , s > 0 \end{cases} \tag{12a}$$

where

$$a_t \equiv \min\left(\frac{1}{2}, \frac{Q \ln C}{\pi t}\right) \tag{12b}$$

and C is the clip, the maximum gain to be applied at any frequency at any time. Compare with equation (5) to verify that clipped IQF is equivalent to unclipped IQF for $1/2 < Q\ln C/\pi t$. The time-variable amplitude spectrum of the clipped IQF for $C = 100$ (40 db) is plotted in Figure 1 for ten different ratios of t/Q.

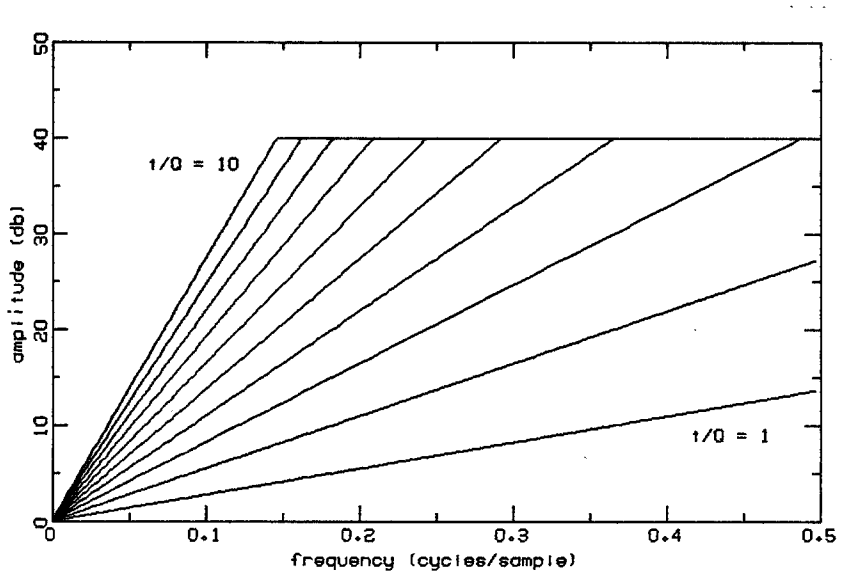

FIG. 1. Time-variable amplitude spectrum, plotted for ten different t/Q, of an inverse Q-filter clipped to a maximum gain of 40 db.

The QAD algorithm is essentially the same with clipping as without, the only difference being that $de_t / d\gamma$ in equation (7) used to compute the perturbation $\Delta\gamma$ should be approximated by

$$\frac{de_t}{d\gamma} \approx \pi t \sum_{s=1}^{\infty} g_{ts}\, e_{t-s}$$

As before, in computing $\Delta\gamma$, one may replace the exponentially damped e_t with the undamped r_t.

Application of Q-adaptive deconvolution to field data

Plotted in Figure 2 is a constant-offset section taken from high-resolution land data. The seismic source was dynamite. The sampling interval is 0.5 msec; the trace length is 500 msec. The recording sampling interval was 0.25 msec. We subsampled the data to reduce storage and computations; spectral analysis of this data revealed little signal content above 600 Hz, even at early traveltimes, so subsampling did not distort the signal band. The data has been corrected for spherical divergence, and static time-shifts have been applied to flatten the event at ≈ 0.17 sec. To enhance the display of late events, exponential gain was applied to the section of Figure 2 to obtain that of Figure 3. To permit close comparison of this section with processed sections, enlargements of the first and last 250 sec of Figure 3 are plotted in Figures 4a and 4b.

The section plotted in Figures 5a and 5b is the result of applying conventional, unit-lag, time-invariant PEF (spiking deconvolution) to the divergence-corrected traces of Figure 2. Each prediction error filter was 12.5 msec (25 samples) long and was computed independently for each trace from the autocorrelation of the entire 500 msec. The output traces have been lowpass filtered after PEF to attenuate frequency components above 600 Hz, and exponential gain has been applied for display as in Figures 4.

Even within the 600Hz frequency band, the data of Figure 5b is far from the "white" output we expect from unit-lag PEF. The attenuation of high-frequencies with increasing traveltime is clearly evident, more so, in fact, on the "deconvolved" section of Figures 5 than on the input section of Figures 4, even though the prediction error filter is time-invariant. This effect is expected whenever the source waveform spectrum is dominated by a few frequency components, as is the case when near surface reverberations (which we include in the term "source waveform") are present. Imagine a seismogram for which the source waveform is a fairly narrowband filter. Prior to deconvolution, attenuation would appear only as an exponential amplitude decay with traveltime. Only after deconvolution of

the source waveform would attenuation yield the event broadening effect seen in Figures 5. Also, the fact that no time-variable gain other than spherical divergence correction was applied to the input traces implies that early events most influenced the design of each prediction error filter; gain applied before PEF might increase the resolution of late events in Figures 5, but only at the expense of over-amplifying high frequencies at early times.

To test the conventional windowing method of handling non-stationarity, we applied PEF to five overlapping windows of each trace in Figure 2. The windows were 150 msec long and, after PEF, were blended linearly in the 62.5 msec overlap. An independent prediction error filter was computed from the autocorrelation of each window of each trace. The output section, with lowpass filtering and exponential gain applied as in Figures 5, is plotted in Figures 6a and 6b.

The differences in Figures 5a and 6a, the first 250 msec, are minor. In the last 250 msec, however, Figure 6b exhibits notably broader frequency bandwidth than does Figure 5b, suggesting that some compensation for attenuation is possible. If a goal of this seismic survey is to finely resolve the deeper reflectors, then Figure 6b is preferable to Figure 5b. Our method of increasing resolution, however, leaves much to be desired. Our chosen window length of 150 msec may or may not be optimal. On the one hand, attenuation may be so severe that a shorter window is desirable. On the other hand, a 150 msec window may already be too short for the 12.5 msec prediction error filters we have used; the filters may be removing "local color" in the reflection coefficients. One can easily find seismograms for which any rule of thumb used to determine the window length breaks down.

QAD represents an alternative to windowing. The section plotted in Figures 7a and 7b was obtained by applying QAD to the divergence-corrected traces of Figure 2. Lowpass filtering was applied as in Figures 5 and 6. Exponential gain was not applied, because QAD, in compensating for attenuation, automatically amplifies the events at late traveltimes whenever the estimated Q is positive. The entire section, with Q^{-1} estimates for each trace, is plotted in Figure 8.

In applying QAD, the length of the prediction error filter was again 12.5 msec; and the IQF was clipped to a maximum gain of 60 db. The final estimate of $\gamma \equiv Q^{-1}$ for each trace was used to start the algorithm for the next trace. The initial estimate for the first trace was $\gamma = 0.01$; estimates for dead traces were left unchanged. Typically, only one iteration per trace was required to converge to $|\Delta\gamma| < 0.0005$.

Comparing time-invariant PEF with QAD, we see little evidence in Figures 7 of the attenuation found in Figures 5. Figure 7b exhibits significantly higher detail in the later events than does Figure 5b. The trace to trace correlation of events in Figures 7 implies that high-frequency signal, not merely ambient noise, has been enhanced by QAD. Comparing

conventional, time-variable PEF with QAD, we again see notably higher resolution in Figures 7 than in Figures 6.

Aside from increasing resolution by compensating for the attenuation of high frequencies, QAD also reduces the frequency dispersion associated with inelastic attenuation. As noted by Robinson (1979), "dispersion effects on field data can create false seismic events as well as mask true events." With this statement in mind, notice the "event" at ≈ 300 msec apparent in both Figures 5b and 6b, but which is much less apparent in Figure 7b.

How meaningful are the Q^{-1} estimates plotted in Figure 8? The well-known similarity between the effects of inelastic attenuation and those of intra-bed multiples implies that our estimate is more or less contaminated by the latter, depending on the unknown reflection coefficients. Furthermore, our estimate remains sensitive to high-frequency, ambient noise neglected in our seismogram model, in spite of our use of clipped IQF. We emphasize, however, that even if the Q^{-1} estimates provided by QAD are only weakly related to inelastic attenuation, these estimates may still be appropriate for deconvolution. Just as the best prediction error filter is, for noisy data, not the inverse of the source waveform, the best Q^{-1} for QAD may not be the true earth Q^{-1}. And if QAD attacks intra-bed multiples along with the effects of inelastic attenuation, so much the better.

Significance of the relatively small, trace-to-trace variations in Q^{-1} estimates could be tested by comparing estimates for different constant-offset sections. These variations, if related to geology, should be independent of source, receiver, or offset coordinates. This test for independence has not been conducted for the data of this paper; a valid test would be difficult because only three or four offsets per midpoint were recorded. The author is currently seeking obviously attenuated seismic data with more offsets available.

Conclusions and future work

Q-adaptive deconvolution offers the following advantages over conventional, time-varying prediction error filtering:

(1) QAD avoids the user-specified windowing or weighting of seismograms.

(2) QAD achieves time-variability by estimating only one more parameter per trace, Q, than does time-invariant PEF. Conventional PEF is made time-varying essentially by estimating more than one "source waveform" per trace.

(3) QAD more effectively compensates for the attenuation of high-frequencies as well as the accompanying dispersion effects.

(4) QAD reduces the need for ad-hoc gain corrections.

(5) QAD provides estimates of Q.

The restriction of QAD to depth-invariant Q^{-1} is unnecessary. Generalization to smoothly depth-variable Q^{-1} will be discussed in a future SEP Report. Also, the author is currently studying the problem of estimating Q (earth Q, not decon Q) from noisy seismograms.

ACKNOWLEDGMENTS

The author is particularly grateful to Fabio Rocca for his suggestion of equation (4) and to Western Geophysical Company for providing the field data used in this study.

REFERENCES

Bracewell, R.N., 1978, The Fourier transform and its applications: New York, McGraw-Hill Book Co., Inc.

Foster, M.R., Sengbush, R.L., and Watson, R.J., 1968, Use of Monte Carlo techniques in optimum design of the deconvolution process: Geophysics, v.33, p.945-949.

Griffiths, L.J., Smolka, F.R., and Trembly, L.D., 1977, Adaptive deconvolution: a new technique for processing time-varying seismic data: Geophysics, v.42, p.742-759.

Hale, D., 1981a, An inverse Q-filter: SEP Report 26, p.231-243.

----- 1981b, Q and adaptive prediction error filters: SEP Report 28, p.209-231.

----- 1981c, Q and Kalman filtering: SEP Report 28, p.233-246.

Lee, D.T.L., Morf, M., and Friedlander, B., 1981, Recursive least squares ladder estimation algorithms: IEEE Trans. Circuits Syst., v.CAS-28, p.467-481.

Robinson, J.C., 1979, A technique for the continuous representation of dispersion in seismic data: Geophysics, v.44, p.1345-1351.

Rocca, F., 1981, Personal communication.

Wang, R.J., 1969, The determination of optimum gate length for time-varying Wiener filtering: Geophysics, v.34, p.683-695.

Widrow, B., 1970, Adaptive filters, in Aspects of network and system theory: New York, Holt, Rinehart and Winston, Inc.

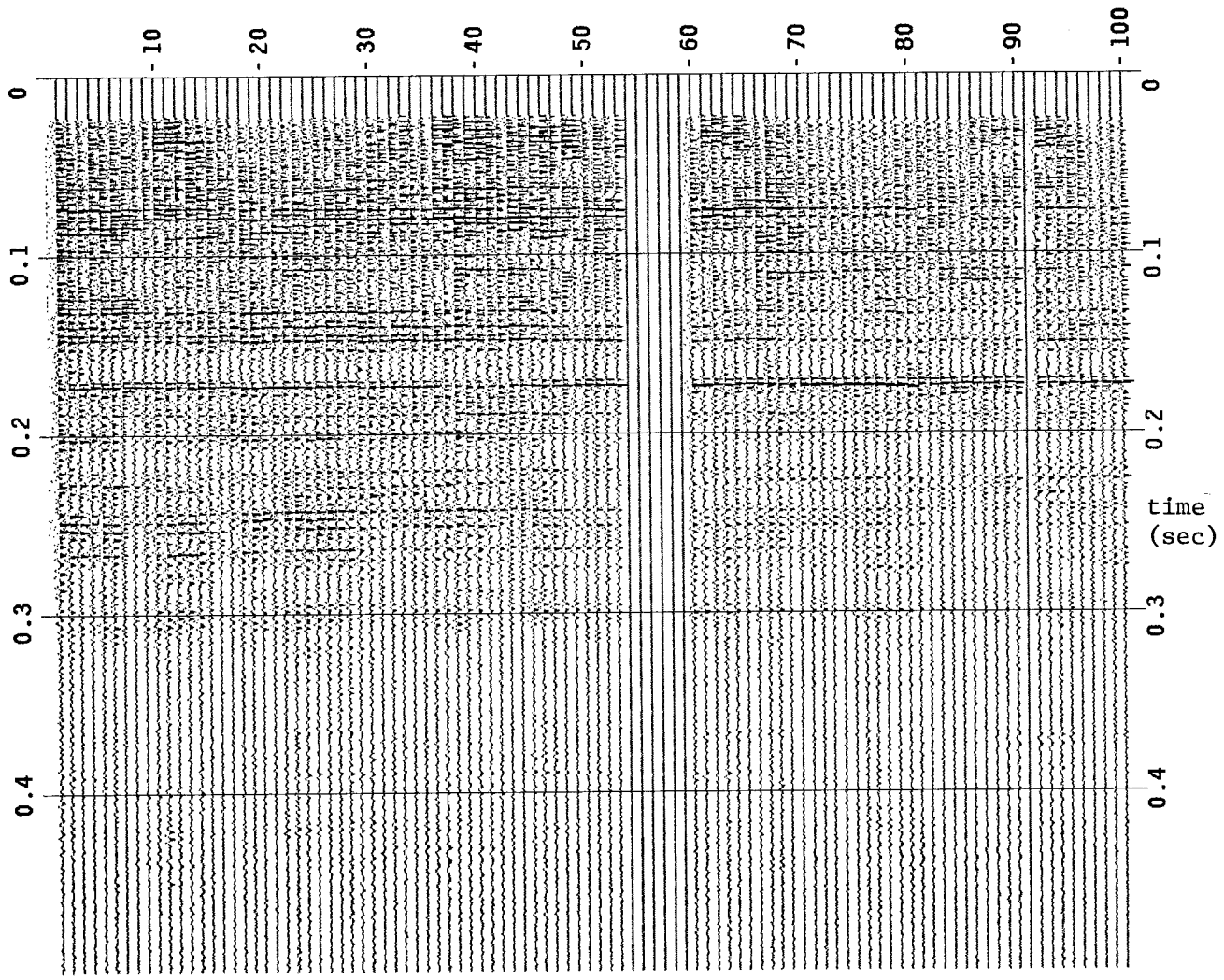

FIG. 2. A constant-offset section of field recorded seismograms used to compare Q-adaptive deconvolution with more conventional, time-varying deconvolution. Spherical divergence and static corrections have been applied.

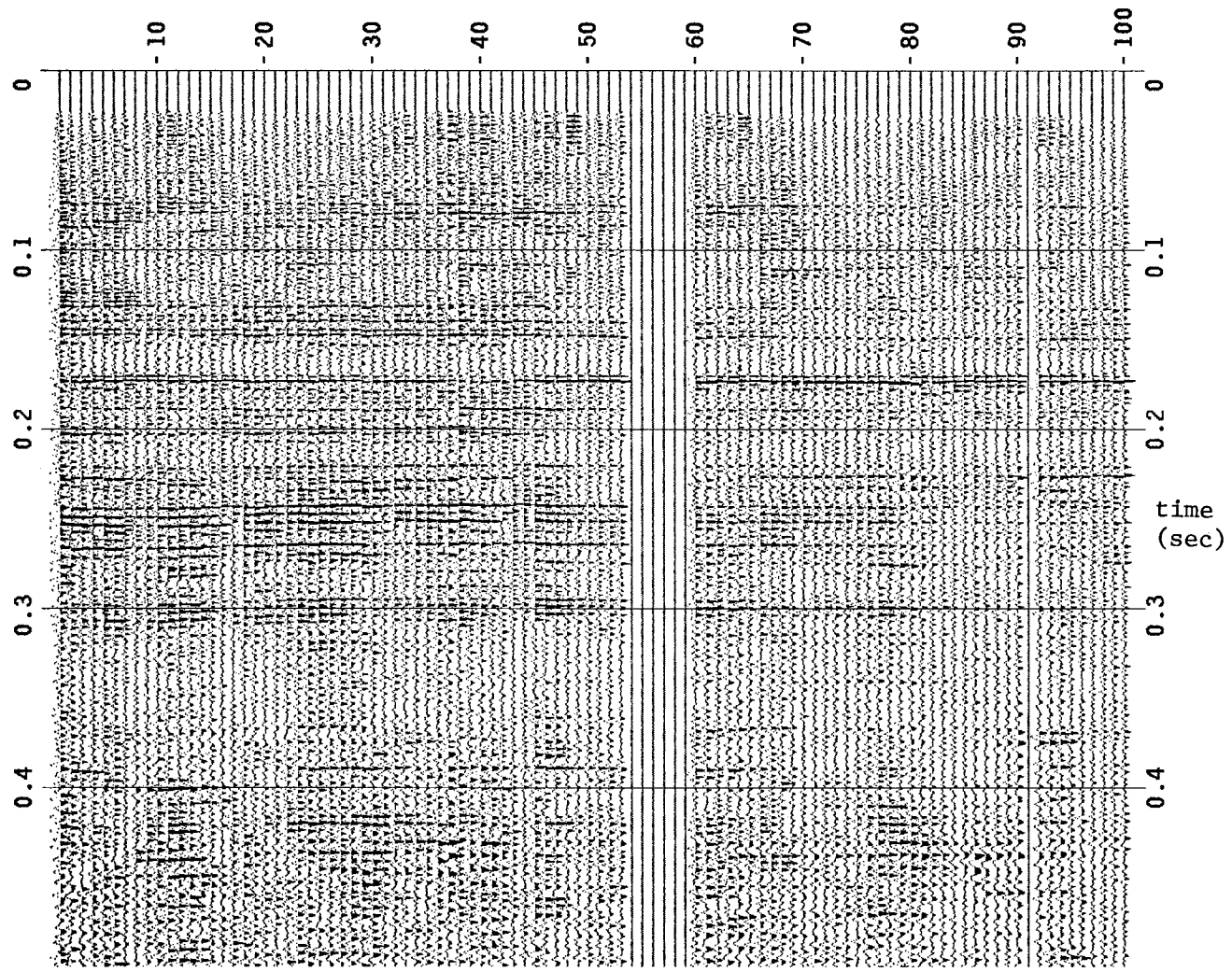

FIG. 3. The section of Figure 2 after exponential gain. $(Figure\ 3)_t = (Figure\ 2)_t * 400^t$.

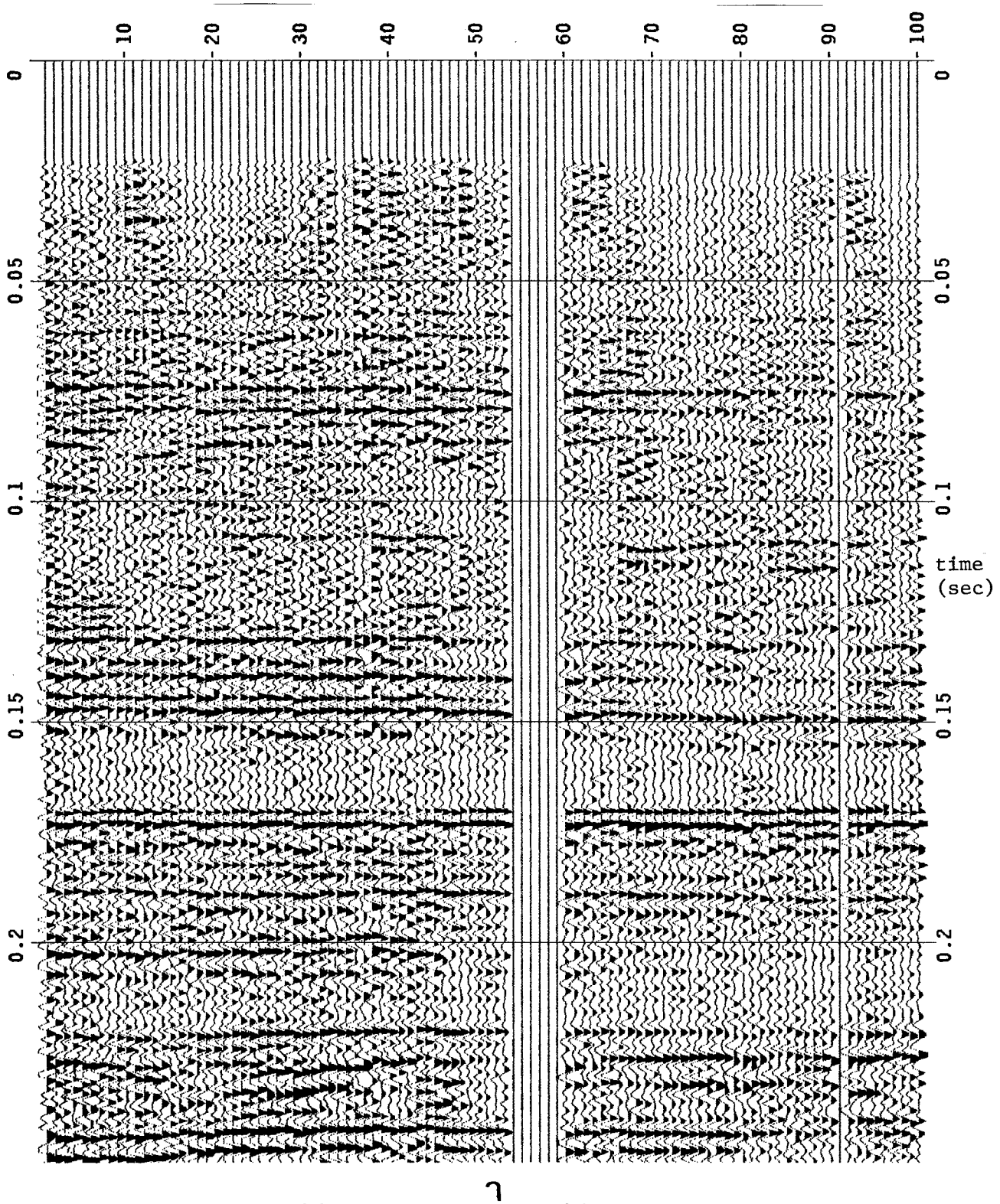

FIG. 4. Enlargement of (a) the first 0.25 sec and (b) the last 0.25 sec of Figure 3.

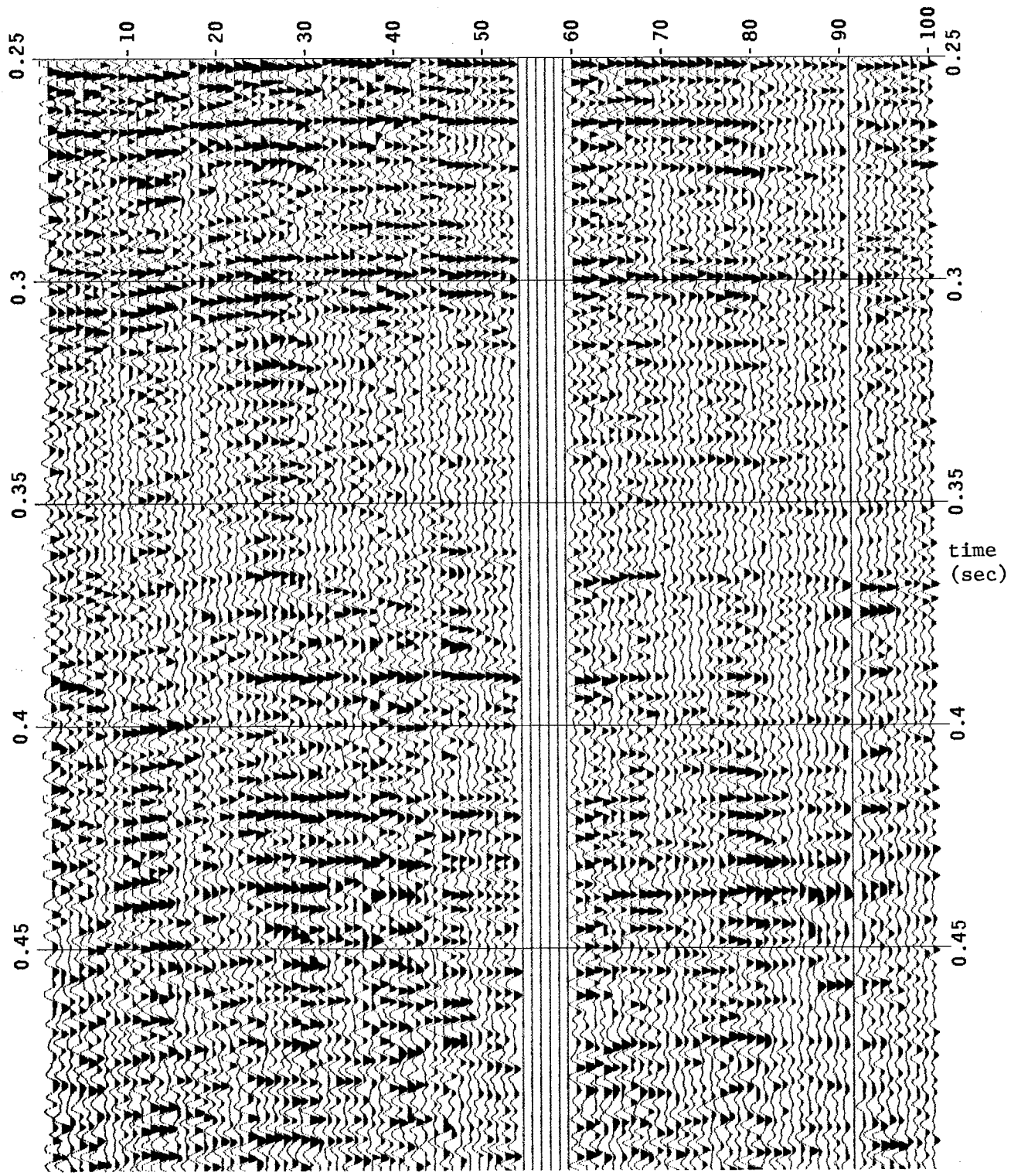

4b

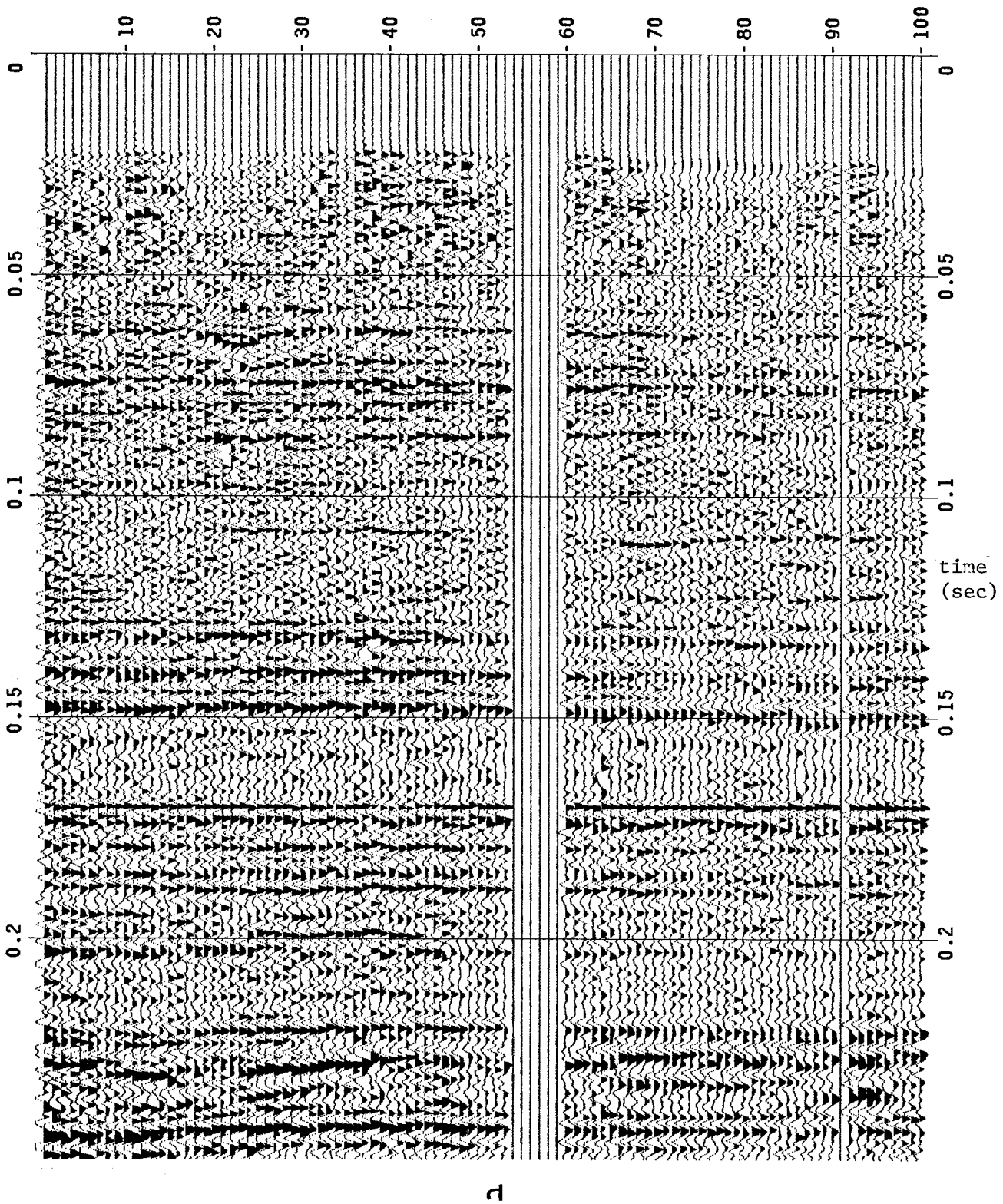

a

FIG. 5. Time-invariant prediction error filtering of the section in Figure 2. Exponential gain and lowpass (to 600 Hz) filtering have also been applied for display of (a) the first 0.25 sec and (b) the last 0.25 sec. Note the loss of resolution with increasing time.

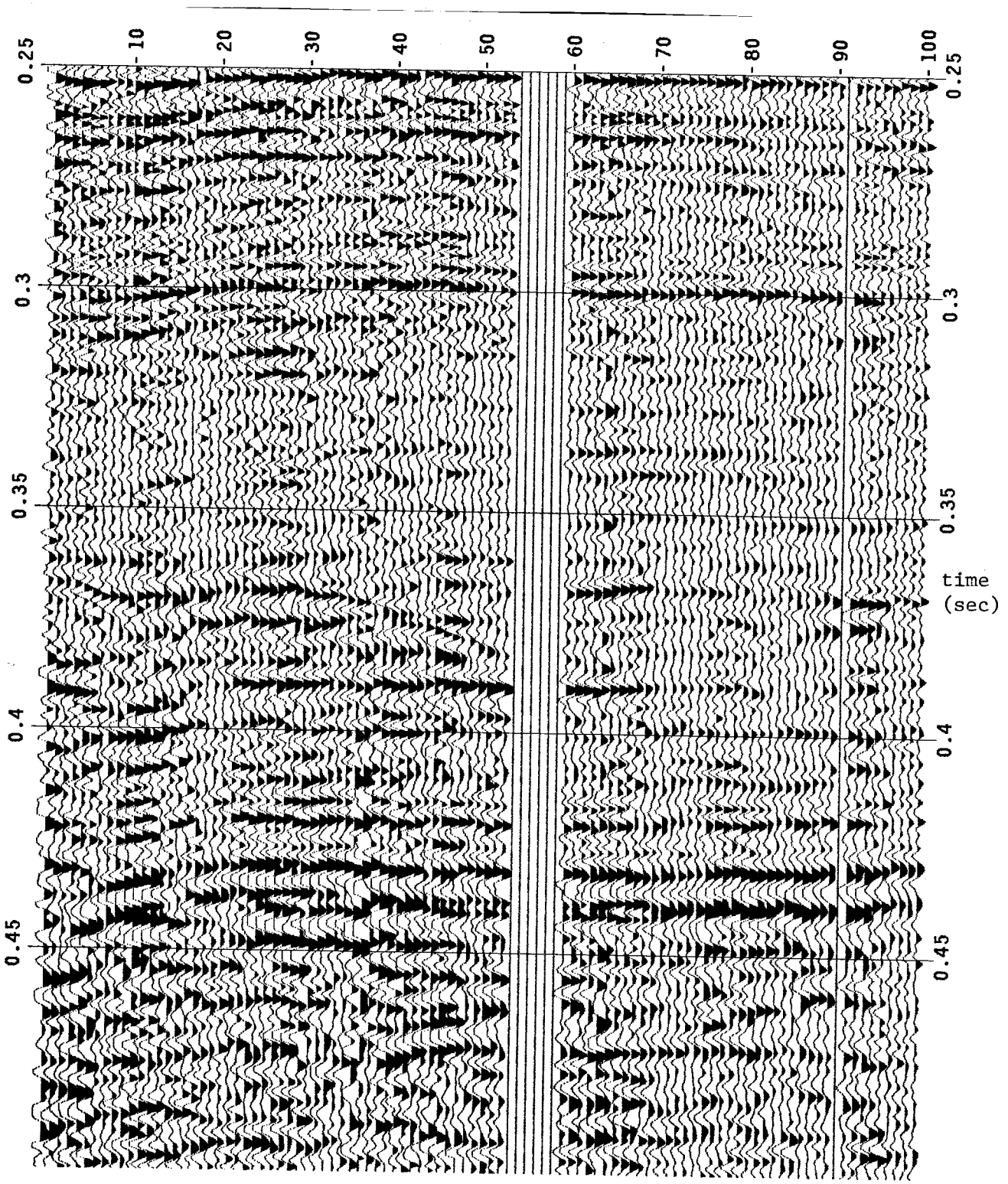

⌜b

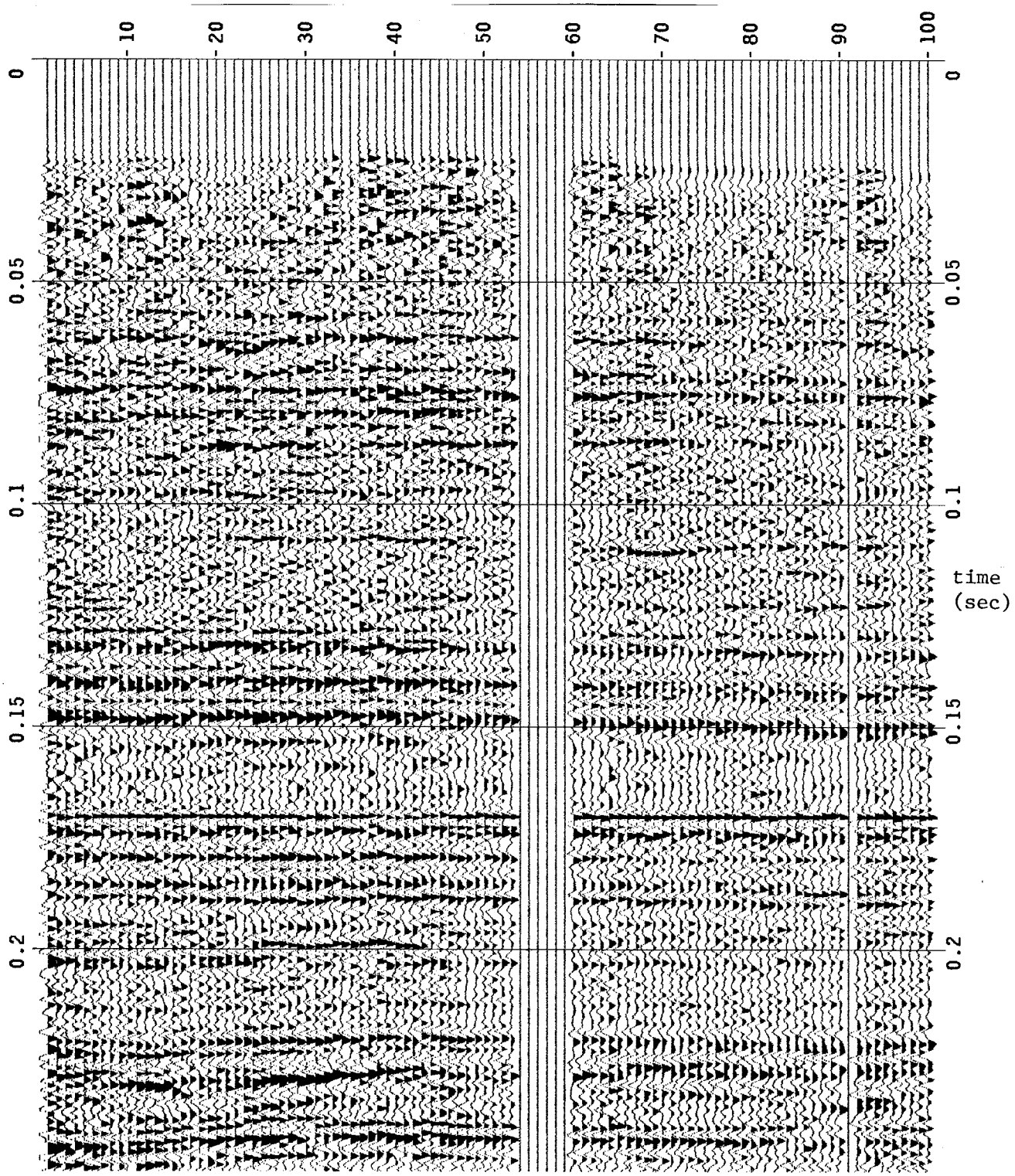

a

FIG. 6. Conventional, time-varying prediction error filtering of the section in Figure 2. Exponential gain and lowpass filtering were applied as in Figure 5 for display of (a) the first 0.25 sec and (b) the last 0.25 sec. Compare the resolution at late times with that in Figure 5b.

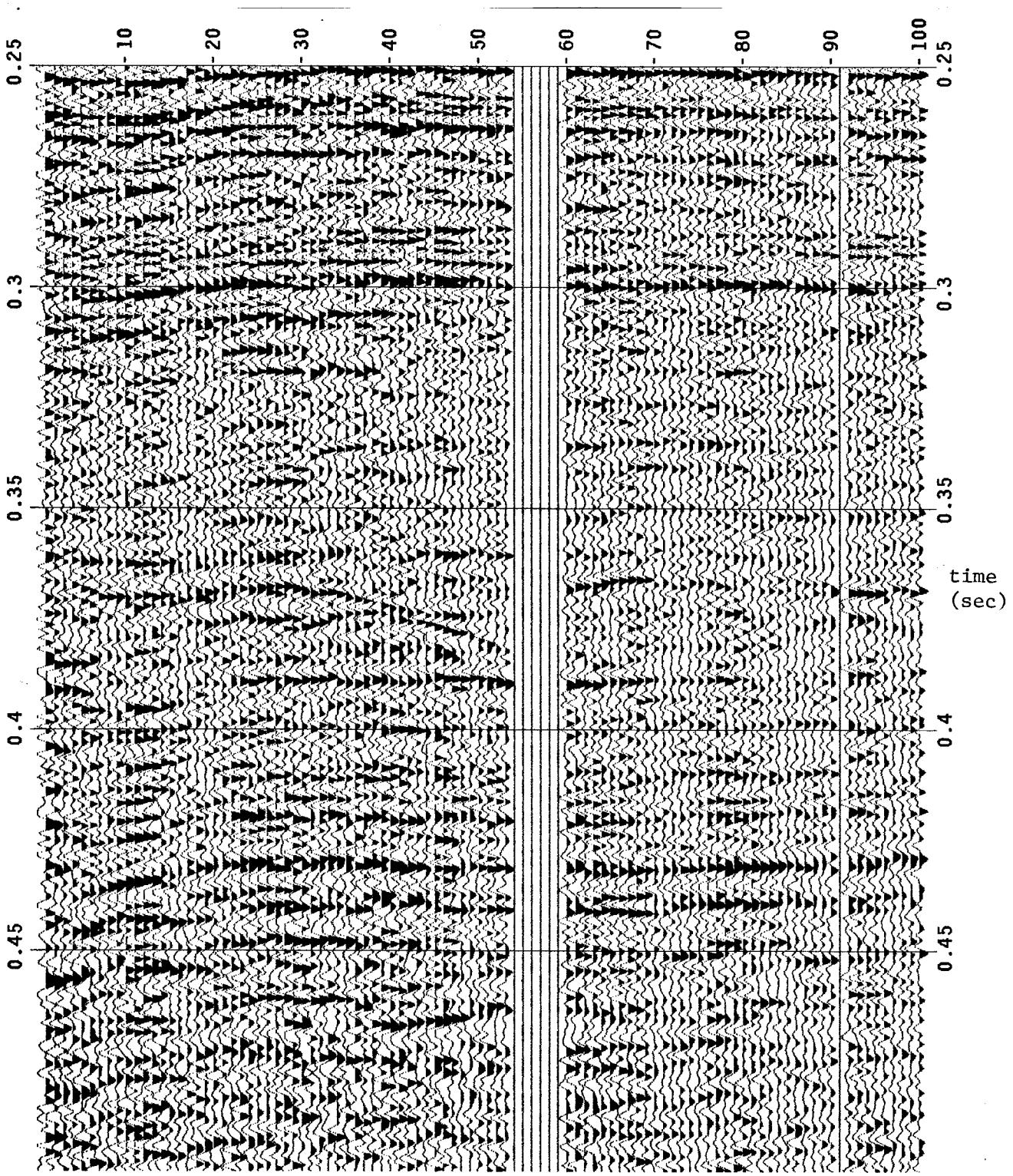

6b

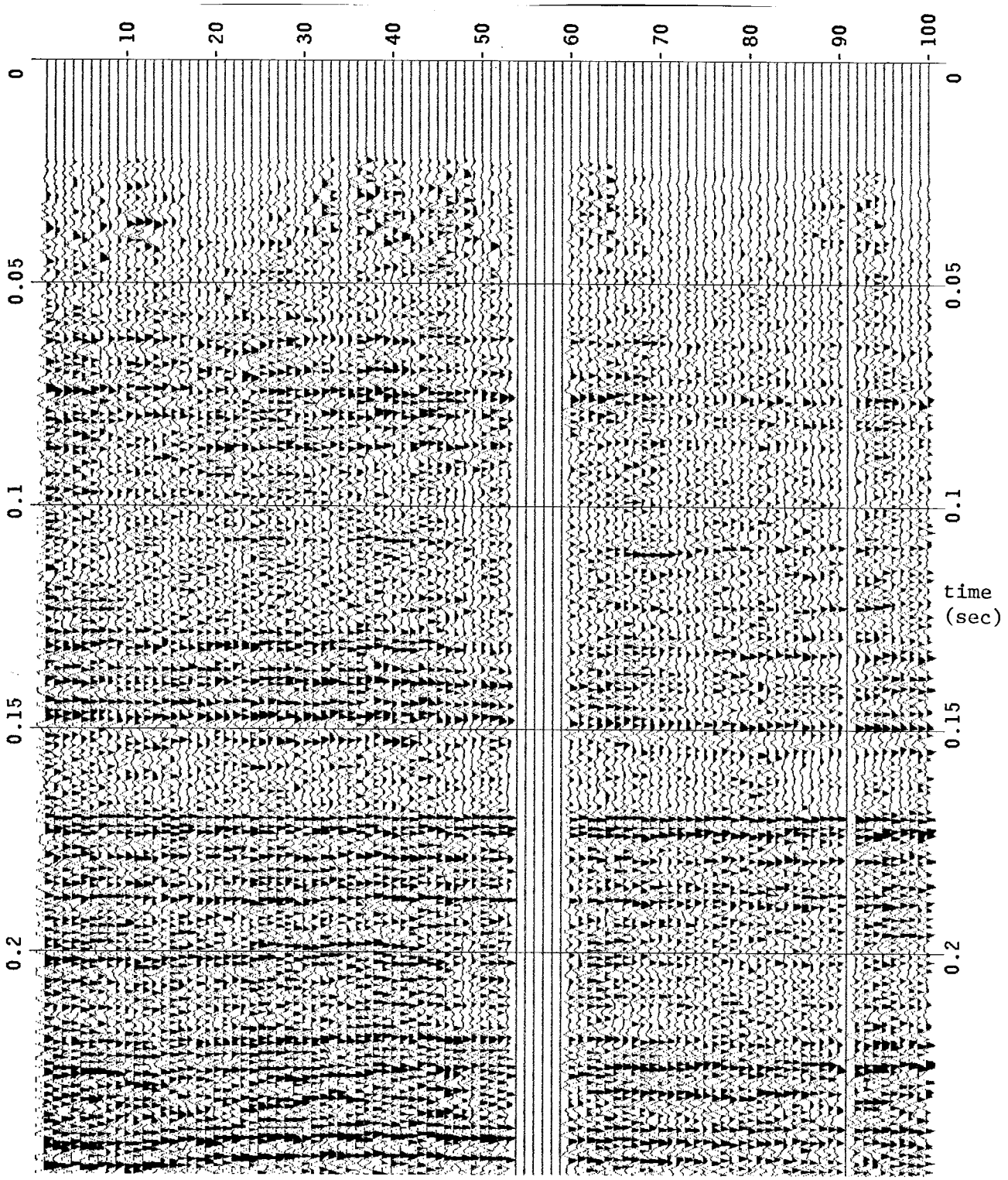

a

FIG. 7. Q-adaptive deconvolution of the section in Figure 2. No exponential gain has been applied. Lowpass filtering was applied as in Figures 5 and 6 for display of (a) the first 0.25 sec and (b) the last 0.25 sec. Note the considerable differences between this section and those of Figures 5 and 6, particularly in last 0.25 where attenuation effects are greatest.

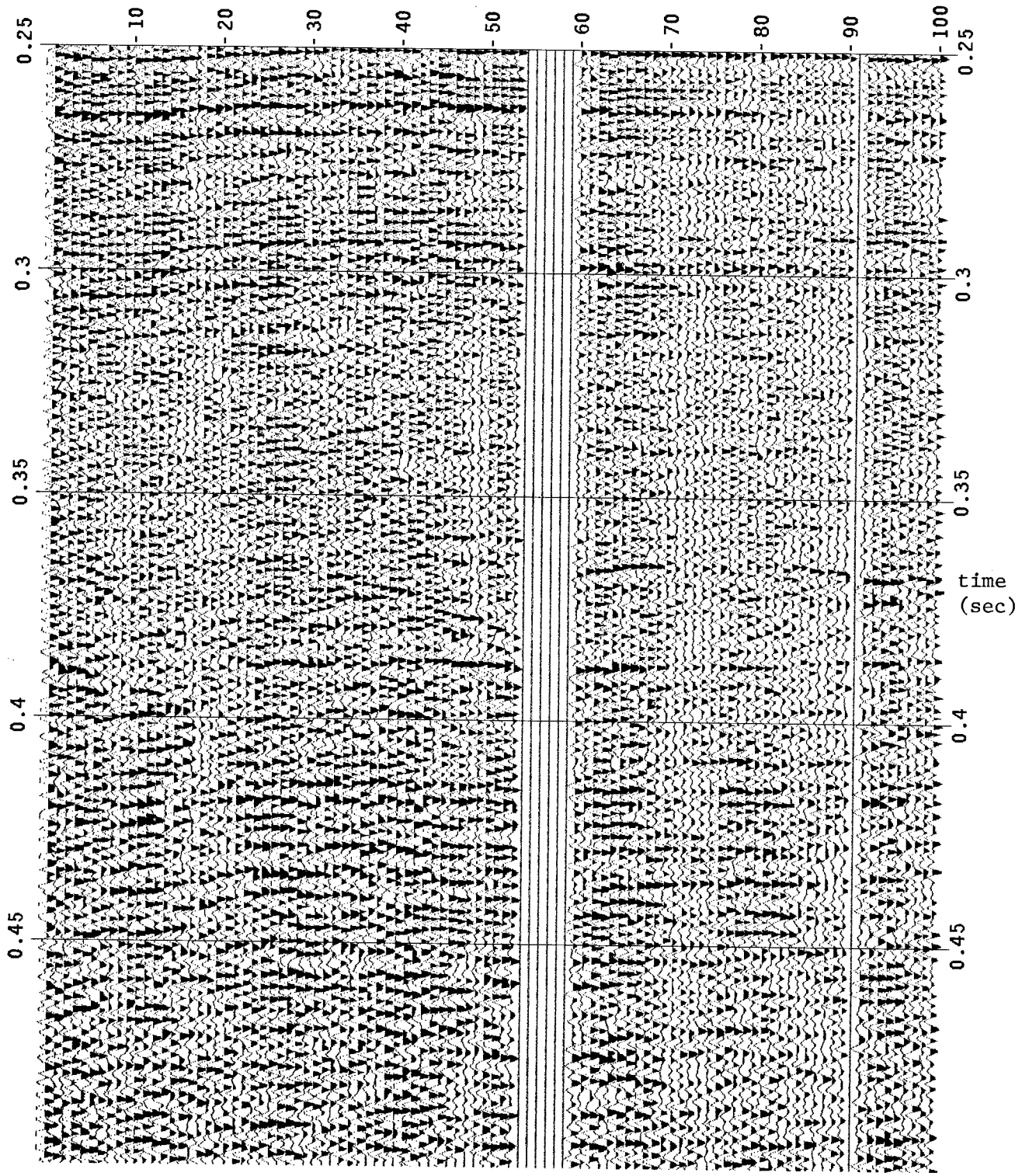

7b

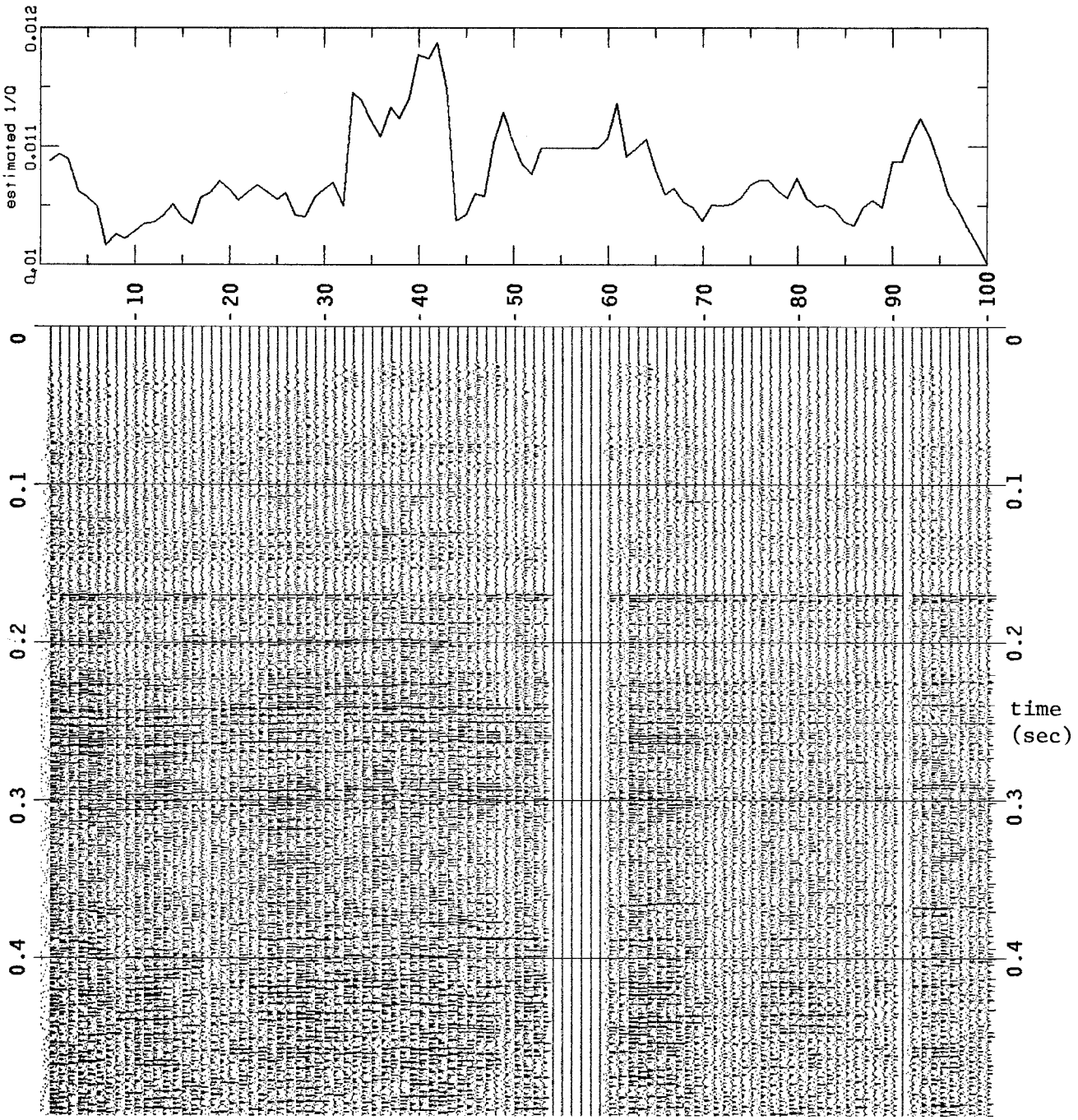

FIG. 8. Q^{-1} estimates for each trace, plotted with the entire Q-adaptive deconvolved section of Figures 7.

Appendix

We seek a discrete representation g_t of the causal filter $g(t)$ having the Fourier transform

$$G(f) = |f| + iH(|f|)$$

To this end, we must constrain the bandwidth of $|f|$ to avoid aliasing g_t as well as to make the Hilbert transform $H(|f|)$ exist. We assume that the sampling interval is unity, and define the real part of the bandwidth constrained $G(f)$ by

$$R(f) \equiv \begin{cases} |f| & , \ |f| < a \\ a & , \ a \le |f| < 1/2 \\ 0 & , \ |f| \ge 1/2 \end{cases}$$

$$\equiv a\Pi(f) - a\Lambda(f/a)$$

where $0 < a < 1/2$, and Π and Λ are the rectangle and triangle functions defined as in Bracewell (1978):

$$\Pi(f) \equiv \begin{cases} 1 & , \ |f| < 1/2 \\ 0 & , \ |f| \ge 1/2 \end{cases}$$

and

$$\Lambda(f) \equiv \Pi(f) * \Pi(f)$$

The significance of the constant a lies in the derivation of clipped IQF. Note presently that, for $a = 1/2$, $R(f)$ equals the real part of $G(f)$ over the interval $-1/2 < f < 1/2$ and equals zero outside this interval. The inverse Fourier transform of $R(f)$ is

$$r(t) = a\,\mathrm{sinc}(t) - a^2\mathrm{sinc}^2(at)$$

which we may sample without fear of aliasing:

$$r_t = \begin{cases} a(1-a) & , \ t = 0 \\ -\sin^2(\pi a t)/(\pi t)^2 & , \ t = \pm 1, \pm 2, \pm 3, \cdots \end{cases}$$

Recalling that a Hilbert transform in the frequency domain is equivalent to multiplication by $\mathrm{sgn}(t)$ in the time domain, the causal filter g_t is easily found from r_t by doubling r_t for $t > 0$ and zeroing r_t for $t < 0$. For $a = 1/2$,

$$g_t = \begin{cases} 1/4 & , \ t = 0 \\ -2/(\pi t)^2 & , \ t = 1,3,5, \cdots \\ 0 & , \ otherwise \end{cases}$$

which is equation (5) in the text.

The derivation of clipped IQF follows from our definition of $R(f)$. Note that $R(f)$ is "clipped" to a maximum value of α. To clip the inverse Q-filter, we place an upper bound C on the amplitude spectrum $\exp[\pi t R(f)/Q]$ by letting α depend on time t:

$$\alpha_t \equiv \min\left(\frac{1}{2}, \frac{Q \ln C}{\pi t}\right)$$

which is equation (12b) in the text. The causal, time-variable filter g_{ts}, where now s denotes the Fourier dual variable to f, is again found by doubling r_s for $s > 0$ and zeroing r_s for $s < 0$:

$$g_{ts} \equiv \begin{cases} 0 & , s < 0 \\ \alpha_t(1-\alpha_t) & , s = 0 \\ -2\sin^2(\pi\alpha_t s)/(\pi s)^2 & , s > 0 \end{cases}$$

which is equation (12a).